Rigidity of epithelial tissues as a double optimization problem

Sadjad Arzash [1,2] Indrajit Tah [3,4] Andrea J. Liu [2] and M. Lisa Manning [1]
[1]Department of Physics, Syracuse University, Syracuse, New York 13244, USA
[2]Department of Physics and Astronomy, University of Pennsylvania, Philadelphia, Pennsylvania 19104, USA
[3]Speciality Glass Division, CSIR–Central Glass and Ceramic Research Institute, Kolkata 700032, India
[4]Academy of Scientific and Innovative Research (AcSIR), Ghaziabad 201 002, India

(Received 22 December 2023; accepted 17 January 2025; published 12 February 2025)

How do cells tune emergent properties at the scale of tissues? One class of such emergent behaviors are rigidity transitions, in which a tissue changes from a solidlike to a fluidlike state or vice versa. Here we introduce a way for a tissue described by a vertex model to tune its rigidity by using "tunable degrees of freedom." We use the vertex model elastic energy as a cost function and the cell stiffnesses, target shapes, and target areas as different sets of degrees of freedom describing cell-cell interactions that can be tuned to minimize the cost function. We show that the rigidity transition is unaffected when cell stiffnesses are treated as tunable degrees of freedom. When preferred shapes or areas are treated as tunable degrees of freedom, however, induced spatial correlations in target cell shapes or areas shift the rigidity transition. These observations suggest that tissues can coordinate changes in cell-scale properties, treated here as tunable degrees of freedom, to achieve desired tissue-scale behaviors.

DOI: 10.1103/PhysRevResearch.7.013157

I. INTRODUCTION

The molecular processes that govern the formation of biological tissues operate at the cellular level but give rise to collective behavior at the multicellular scale. Similarly, in systems such as mechanical, flow, or electrical networks instructions encoded in the microscopic structure control collective properties. In materials design, the process of achieving a specific functionality typically involves a series of iterative steps in which the system is continually tested for desired functionality, adjusted based on feedback, and tested again to refine its performance. An effective strategy for solving this inverse problem of material design in these systems is gradient descent on a *cost function* that embodies the desired collective property by tuning microscopic *tunable degrees of freedom* (DOFs) characterizing interactions, such as the presence or absence of a bond [1–4], bond stiffnesses [5,6], or rest lengths in elastic networks, or conductances [5] in flow or electrical networks. Physics dictates that each system must also satisfy physical constraints during this process, imposed by minimizing the energy in elastic networks or dissipated power in flow or electrical networks, with respect to *physical DOFs* (node positions in elastic networks or node pressures/voltages in flow/electrical networks).

Simultaneous minimization of the cost function and energy/power with respect to tunable and physical DOFs (*double optimization*) can be used to generate an auxetic [1,3,4] or allosteric response [2,5]. Alternatively, minimization of the energy/power while varying tunable DOFs according to local rules [7] can also be effective. Such local update rules include those that naturally occur in real materials, like directed aging [6,8,9], as well as rules that approximate gradient descent, as in Equilibrium Propagation [10] or Coupled Learning [11]. These ideas have led to successful learning of desired properties in the laboratory [2,6,8,12–14].

Here we show that biological tissues can potentially tune cell-scale properties, viewed as tunable DOFs, to drive robust macroscopic, collective behaviors necessary for development and evolution. Our work focuses on rigidity transitions, which are a specific example of macroscopic collective behavior. Rigidity transitions occur when the tissue collectively switches back and forth from fluidlike behavior, where cells are able to rearrange neighbors and the tissue can accommodate significant strain, to a solidlike behavior, where cells do not change neighbors and straining the tissue costs energy. Recent experiments demonstrate that tissues shift from a solid to a fluid [15,16] or near-fluid state [17] as a function of space [15] and time [16], to facilitate flows necessary for body axis elongation [15–17] and organ formation [18,19]. A well-vetted class of simple biophysical models (vertex [20–23], Voronoi [24], and cellular Potts [25] models) have successfully made quantitative predictions—with no fit parameters—for rigidity transitions in confluent epithelial tissues [16,22,26]. A key feature of vertex models, validated in experiments, is that the rigidity transition is controlled by a geometric cell shape factor. This shape factor serves as a coarse-grained parameter that encapsulates the effects of molecular-scale processes, such as contractility driven by myosin and adhesion regulated by E-cadherin [27,28].

In this paper we explore the idea that developmental processes can usefully be regarded as double optimization processes, in which cell-scale tunable DOFs, such as cell shape, are adjusted to optimize a tissue-scale cost function that is minimized when the tissue achieves a desired macroscopic final state, while simultaneously staying in mechanical equilibrium. This viewpoint is bolstered by the recent finding that the *Drosophila* amnioserosa appears to shift its rigidity transition to remain rigid throughout the developmental process of dorsal closure by tuning preferred cell shapes continuously throughout the process [29]. By framing a developmental process as a double optimization problem, we can unambiguously identify which cell-scale parameters within a vertex model are important for controlling a given macroscopic property. We argue that double optimization represents a theoretical framework for identifying cell-scale and molecular mechanisms that control larger-scale behavior, which is a major open problem in cell and developmental biology. This framework allows us to study an *ensemble* of tissue states that all minimize the same cost function. If we can identify common features in this ensemble that emerge from the double optimization process, we can then search for such features in biological experiments.

This problem is also interesting from a physics perspective. Previous work has focused on over-constrained networks or jammed packings, in which the parameter that controls rigidity is the coordination number that describes the number of constraints per particle or node. This is because such systems become rigid when the number of DOFs equals the number of constraints. Work by Hagh *et al.* [30] introduced tunable DOFs in the form of particle radii and showed that these can be used to control rigidity over a wide range by tuning the coordination number, enabling the design of highly stable jammed states [30].

In contrast, vertex models are highly under-constrained, i.e., the number of physical DOFs (vertex positions) is much larger than the number of constraints. Vertex models become rigid through geometric incompatibility, where cells are unable to achieve their target perimeters and areas. The system is stabilized due to energetic costs that occur only at second order in perturbations to the constraints [31], the same mechanism that drives strain-induced rigidity in subisostatic fiber networks [32–35]. This raises the question of whether rigidity can be controlled in vertex models using tunable DOFs.

As a first step towards addressing these open physics and biology questions, we investigate tunable DOFs in 2D vertex models. We study how different sets of allowed tunable DOFs—specifically, cell stiffnesses, preferred areas, or preferred perimeters—affect our ability to minimize a cost function. Here, as proof of principle, we make the simplest possible choice, analogous to Ref. [30] for the cost function jammed packings: the total mechanical energy of the system. In other words, we explore the ability of different sets of tunable DOFs to drive the system towards zero-energy floppy/fluidized states.

To characterize the sensitivity of vertex models to tunable DOFs, we must also account for an important consideration. Such models can be driven towards a fluidlike state by simply altering the mean [23] or the width [36] of the distribution of cell shapes. A similar result was discovered in over-constrained jammed packings, where rigidity was found to be trivially dependent on the first and second moments of the radii distribution [30]. As in that previous work [30], we avoid these trivial dependencies by fixing the distribution (or a set of its moments) and asking whether double optimization is able to introduce *spatial correlations* in the tunable DOFs that are sufficient to shift the rigidity transition. If the system is able to learn, our next goal is to identify which tunable DOFs are able to control the rigidity transition, and identify observable features that distinguish states that have learned from those that have not.

II. MODEL

We study a 2D vertex model [21,37], which describes a tissue monolayer as a network of polygonal cells. The physical DOFs are the polygon vertices. Cellular properties and interactions are encoded in an energy function $E = \sum_i^N [K_{A,i}(A_i - A_{0,i})^2 + K_{P,i}(P_i - P_{0,i})^2]$, where A_i and $A_{0,i}$ are the actual and preferred areas, P_i and $P_{0,i}$ are the actual and preferred perimeters, and $K_{A,i}$ and $K_{P,i}$ are the area and perimeter moduli of cell i. It is helpful to make the above equation dimensionless using $\langle K_{A,i}\rangle \langle A_{0,i}\rangle^2$ as the units of energy and $\sqrt{\langle A_{0,i}\rangle}$ as the units of length. We then have

$$e = \sum_i^N [k_{a,i}(a_i - a_{0,i})^2 + k_{p,i}(p_i - p_{0,i})^2], \tag{1}$$

where $\langle k_{a,i}\rangle = 1$, $\langle a_{0,i}\rangle = 1$, and p_i, $p_{0,i}$ are the dimensionless actual and preferred shape indices. Equation (1) has been well studied for the case where $k_{a,i}$, $a_{0,i}$, $k_{p,i}$ have delta-function distributions, and $p_{0,i}$ has a distribution of zero [21,23,24] or nonzero width [36]. Here we study Eq. (1) using the open-source CellGPU code [38], promoting $k_{a,i}$, $a_{0,i}$, $k_{p,i}$, and $p_{0,i}$ to tunable DOFs. Initially, N cell centers are set by random sequential addition in a square box with length $L = \sqrt{N}$; vertices and edges are defined from a Voronoi tessellation of these points. The energy in Eq. (1) is minimized using the FIRE algorithm [39].

We investigate the impact of various sets of tunable DOFs separately; e.g., when $p_{0,i}$ are tunable DOFs, we initialize p_{0i} values from a Gaussian distribution with mean $\langle p_{0i}\rangle$ and standard deviation σ, and set $k_{a,i} = k_{p,i} = a_{0,i} = 1$ for all cells. As in Hagh *et al.* [30], we focus on the case where the cost function is simply the energy, or the physical cost function. Hagh *et al.* have shown that in sphere packings, minimizing the energy with respect to both physical DOFs (particle positions) and tunable DOFs (particle radii) allows the system to find very rare low-energy states [30], shifting the jamming transition. We minimize the energy (Eq. (1)) with respect to both physical DOFs (vertex positions) and tunable DOFs to study the influence of tunable DOFs on the rigidity transition. We keep the tunable DOF distributions approximately fixed by imposing constraints on sets of moments of the distribution, such as the $m = \{-1, -2, -3, 1, 2, 3\}$ moments [see the Supplemental Material (SM) [40]]. This constrained minimization method ensures the distribution of tunable DOFs stays fixed during our minimization dynamics. We also perform zero-temperature swap minimization to fix the distribution exactly. In this method, each of the N cells

maintains its preferred property (introducing N constraints), cells are swapped in a trial move, and moves that lower the energy are accepted (see SM [40]).

We evaluate rigidity based on the shear modulus G [41]: $G > 0$ in the rigid phase, and $G = 0$ in the fluid phase. To compute G, we freeze all tunable DOFs (see SM [40]). Unless otherwise stated, error bars show the standard deviation over 50 samples.

III. RESULTS

A. Introducing target shapes and areas as tunable DOFs can fluidize tissues

As the preferred shape index p_0 increases, confluent tissues with only physical DOFs experience a solid-fluid phase transition at a critical value p_0^* [23,34]. For systems with polydisperse $p_{0,i}$, the critical point p_0^* shifts towards larger average preferred shape factors with increasing standard deviation σ of the p_0 distribution [36] [black data in Fig. 3(a)]. For a system with $p_{0,i}$ drawn from a Gaussian distribution with $\sigma = 0.2$ [16], we find $p_0^* = 4.05 \pm 0.02$ [the curve with black circles in Fig. 1(a)]. As $p_0 \to p_0^{*-}$, approaching the transition from the rigid side, the shear modulus vanishes as a power law: $G \approx a(p_0^* - p_0)^b$ with $b = 1.0$ [23,34]. We subtract a finite-size-effect offset (see SM [40]) and fit to this form to see how the scaling exponent b and the position of the rigidity transition, p_0^*, change as we introduce different sets of tunable DOFs.

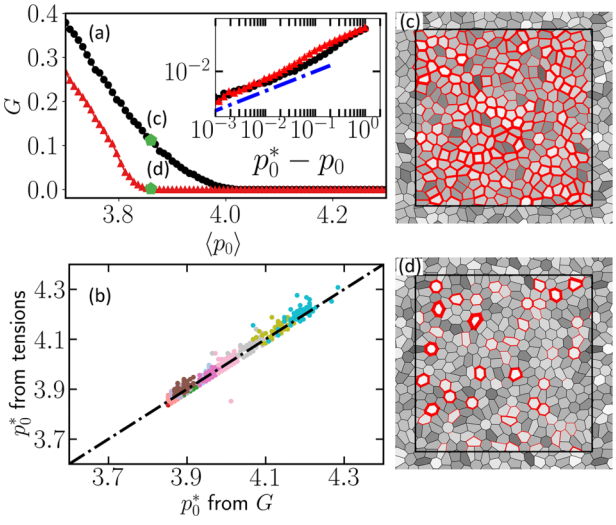

FIG. 1. (a) Shear modulus G versus average target shape $\langle p_0 \rangle$ in vertex models with polydisperse p_{0i}. The black curve (circles) shows minimization based solely on physical DOFs, while the red curve (triangles) includes both physical and $\{p_{0i}\}$ DOFs. Inset illustrates shear modulus scaling; the dashed blue line indicates a slope of 1.0. (b) Rigidity transition point p_0^* from edge tension percolation versus shear modulus G with different σ values for $\{p_{0,i}\}$ as DOFs. The black dashed line represents $y = x$. (c), (d) Tissue structures for highlighted points in (a). Cells are colored based on their $p_{0,i}$ values (higher $p_{0,i}$ is darker). Edge tensions are shown in red, with thickness proportional to tension. Both snapshots have the same distribution of target shape factors $\{p_{0,i}\}$.

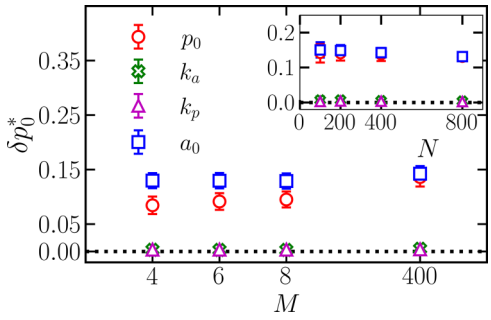

FIG. 2. Change in the rigidity transition point δp_0^* after introducing different transient DOFs (different symbols), as a function of the number of moment constraints M on the distribution. Specifically, the exact moments for M constraints are $\{-M/2, \ldots, M/2\}$, excluding zero. Inset shows how δp_0^* varies with N for $M = 400$. The zero-temperature swap system is indicated by 400 constraints, the number of cells in the tissue. These results correspond to a standard deviation of $\sigma = 0.2$ of transient DOFs.

Rigidity is associated with percolation of edges (cell-cell junctions) with nonzero tensions [36]. The tension of edge ij separating cells i and j is $T_{ij} = 2K_{P,i}(P_i - P_{0,i}) + 2K_{P,j}(P_j - P_{0,j})$, which when nondimensionalized becomes

$$t_{ij} = 2k_{p,i}\sqrt{a_{0,i}}\tau_i^p + 2k_{p,j}\sqrt{a_{0,j}}\tau_j^p, \tag{2}$$

where $\tau_i^p = p_i - p_{0,i}$ is the tension of cell i in units of $\langle K_{A,i}\rangle\langle A_{0,i}\rangle^{3/2}$, i.e., energy/length. For $p_0 < p_0^*$, a percolating cluster of nonzero edge tensions (Fig. 1) maintains mechanical rigidity of tissue [36]. For $p_0 > p_0^*$, nonzero edge tensions fail to percolate and the tissue is fluid—it cannot resist shear deformation.

We first note that p_0^* is unaffected when the cell perimeter stiffnesses $\{k_{p,i}\}$ in Eq. (1) are allowed as tunable DOFs (Fig. 2). This observation is consistent with the fact that, in the case of uniform $\{p_{0,i}\}$, the deviations in perimeter $\tau_i^p = p_i - p_{0,i}$ are geometrically constrained to be non-negative in the solid phase, which prevents the stiffness DOFs $\{k_{p,i}\}$ from altering the percolation of edge tensions. This result aligns with prior studies of jamming in sphere packings [30], where stiffness DOFs are similarly irrelevant in shifting the transition point. While this observation is supported by our numerical results, a rigorous mathematical proof of this effect is nontrivial and is reserved for future investigation. The scaling exponent b also remains unchanged but the tissue softens (see SM [40]).

We next consider variations in cell area stiffnesses $k_{a,i}$ as tunable DOFs with $a_{0,i} = 1$, $k_{p,i} = 1$ and $p_{0,i} = p_0$ for every cell i. One might expect the system to distribute its cell areas a_i to be closer to $a_{0,i} = 1$ for cells with larger values of $k_{a,i}$, leading to correlations that shift the transition. However, vertex models are unstressed at the rigidity transition [31], so their properties there cannot depend on $k_{a,i}$. As a result, the rigidity transition is unaffected by introducing $k_{a,i}$ as tunable DOFs.

We now consider preferred shape indices $\{p_{0,i}\}$ as tunable DOFs. Upon minimization, tissues adjust the values of some individual preferred shape indices $p_{0,i}$ to lower the energy by eliminating $p_i - p_{0,i}$. This leads to a lower fraction of nonzero

tension edges, shifting the rigidity transition p_0^* to lower values [red triangles in Fig. 1(a)]. Since typical shape indices observed in experiments range from about 3.8 to 4.3 [16,22], the shift in the transition point from about 3.85 to about 4 is quite significant. Thus, minimizing E with respect to $p_{0,i}$ as well as the vertex positions introduces spatial correlations in $p_{0,i}$ that fluidize a tissue that would otherwise be solid. This shift persists whether we constrain certain moments of the p_0 distribution or preserve the distribution exactly (see Fig. 2). The scaling exponent b for the shear modulus remains unaffected within our error bars (see SM [40]). Moreover, the amplitude a of the shear modulus decreases more than when $k_{p,i}$ or $k_{a,i}$ are tunable DOFs (see SM [40]).

Since allowing shape indices as DOFs shifts p_0^*, we expect that it also alters the vibrational density of states that describes the curvatures of the potential energy landscape in the rigid phase near p_0^*. As shown in the SM [40], double optimization on the $\{p_{0,i}\}$ DOFs reduces the curvatures and shifts the normal modes to lower frequencies. While previous work has suggested that additional signatures of double optimization, such as high-curvature directions in the cost function [42,43], can be found in eigenmodes of the cost Hessian, which in this case are identical to the vibrational normal modes since the cost function is simply the energy, we do not find any such signatures here. We conjecture that this is because the cost landscape and physical landscapes are already identical from the beginning of the double optimization process. As a result, there is no way in which double optimization can leave imprints on the energy landscape through coupling of two distinct landscapes.

Allowing $p_{0,i}$ as tunable DOFs not only shifts p_0^* but also increases the amount of structural order in the tissue (see SM [40]). This ordering feature can be seen by sharper peaks in the pair correlation function. Consistent with this observation, we find a higher fraction of hexagonal cells f_6 when $\{p_{0,i}\}$ are added as new DOFs (see SM [40]). Importantly, the range of f_6, from 0.3 to 0.65, is tunable through adjustments in the mean and standard deviation of the $\{p_{0,i}\}$ distribution. This property can be used to mimic the level of hexagonal cells in epithelial tissues, which has been shown to change substantially between different stages of development [44].

B. Nonmonotonic relationship between rigidity shift and distribution width

So far we have used a fixed standard deviation ($\sigma = 0.2$) for the distribution of $\{p_{0,i}\}$. However, σ significantly influences tissue rigidity [36], shifting p_0^* upwards [36] [black circles in Fig. 3(a)]. This raises the question: how does the shift in the transition p_0^* due to adding $p_{0,i}$ as tunable DOFs vary with σ? We observe a reduction in p_0^* at all σ [compare the red triangles to black circles in Fig. 3(a)]. Interestingly, the magnitude of this reduction is nonmonotonic. The purple curve in Fig. 3(a), δp_0^*, shows that the shift in the transition is maximal at $\sigma \approx 0.15$. This suggests there is an optimal level of cell-to-cell fluctuations in biological tissues that enables double optimization to modulate rigidity.

To understand this nonmonotonicity, we first note that as σ approaches zero, the $\{p_{0,i}\}$ distribution approaches a delta function and there are no tunable DOFs. Therefore, δp_0^* must

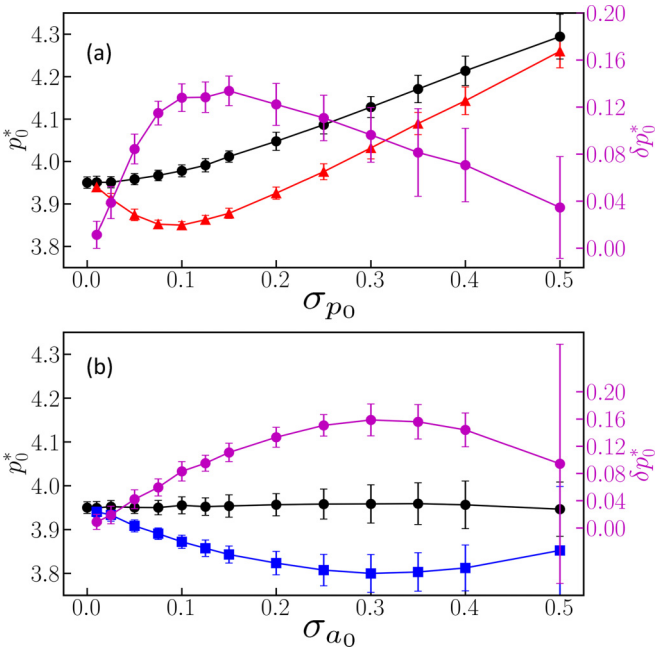

FIG. 3. The effect of polydispersity of tunable DOF distributions on the rigidity transition point. (a) The left axis shows the transition point p_0^* versus the standard deviation σ_{p_0} of the $\{p_{0,i}\}$ distribution. When only vertex positions can vary during energy minimization (black circles), p_0^* increases with σ_{p_0}. However, when $\{p_{0,i}\}$ are also allowed to vary (red triangles), the behavior of p_0^* versus σ_{p_0} becomes nonmonotonic. The right axis δp_0^* shows the reduction of p_0^* due to adding $\{p_{0,i}\}$ as DOFs. (b) Same as (a), but with $\{a_{0,i}\}$ allowed to vary instead of $\{p_{0,i}\}$.

increase away from that point. To understand why δp_0^* decreases for $\sigma \gtrsim 0.15$, we analyzed the correlations between p and p_0 across all cells, both with and without p_0 as tunable DOFs. As expected, the Pearson's correlation coefficient $\rho(p, p_0)$ rises when we incorporate cell p_0 values as tunable DOFs across all σ values (see SM [40]); the energy is lowered by bringing p_i closer to $p_{0,i}$. But for $\sigma \gtrsim 0.15$, p and p_0 already exhibit strong correlations even when $p_{0,i}$ are not tunable DOFs. Introducing $p_{0,i}$ as tunable DOFs only marginally enhances this correlation, so δp_0^* decreases as shown in Fig. 3.

Finally, we consider the preferred cell areas, $A_{0,i}$. In tissues where $A_{0,i} = A_0$ is the same for all cells, altering A_0 while keeping P_0 fixed does not affect p_0^* due to the confluency constraint ($\sum A_i = \text{constant} = L^2$) [45,46]. Yang *et al.* [45] found that the difference between A_0 and the actual area $\langle A \rangle = N/L^2$ alters the overall pressure of the system, but not the shear stresses. We find that even in the presence of heterogeneous $A_{0,i}$ values, p_0^* is unaffected by changes in the *average* target area $\langle A_0 \rangle$ (see SM [40]), so in what follows we hold $\langle A_0 \rangle = 1$ fixed. The solid black circles in Fig. 3(b) shows that varying the *width* of the distribution of the dimensionless $a_{0,i}$ in Eq. (1) also does not affect the transition point. Note that defining target shape factors as $P_{0,i}/\langle A_i \rangle$ would introduce variability in the transition point with σ_{a_0} (see SM [40]). This suggests that the enhanced rigidity discussed in Ref. [36] is caused by heterogeneity in target shape indices ($p_{0,i} = P_{0,i}/\sqrt{A_{0,i}}$) and not by heterogeneity in $P_{0,i}$.

Given these results, we promote $\{A_{0,i}\}$ to tunable DOFs while keeping $\langle A_{0,i}\rangle$ fixed. This introduces *two* sets of tunable DOFs in the dimensionless energy in Eq. (1), namely $\{a_{0,i}\}$ and $\{p_{0,i}\}$. We have already shown how introducing $\{p_{0,i}\}$ as tunable DOFs affects rigidity, so now we consider the effects of $a_{0,i}$ in isolation. To do so, we maintain a constant target shape factor for cells, i.e., $p_{0,i} = p_0$, by coupling the target perimeters $\{P_{0,i}\}$ with the target areas, $\{P_{0,i} = p_0\sqrt{A_{0,i}}\}$. This allows us to consider only $\{a_{0,i}\}$ while keeping the average $\langle A_{0,i}\rangle = 1.0$ at homogeneous $p_{0,i} = p_0$. We find that introducing $\{a_{0,i}\}$ as tunable DOFs leaves the scaling exponent for the shear modulus unchanged (see SM [40]). Similar to $\{p_{0,i}\}$, the $\{a_{0,i}\}$ tunable DOFs shift the transition downwards. This occurs at all values of the width of $\{a_{0,i}\}$ distribution, σ_{a_0}, with the maximum shift occurring around $\sigma_{a_0} \approx 0.3$. Correlations in $a_{0,i}$ from cell to cell causes τ_{ij} in Eq. (2) to vanish for some edges, shifting the percolation of nonzero tensions to lower p_0^*.

IV. DISCUSSION

We have explored the effects of adding tunable DOFs in 2D vertex models on the rigidity transition point, p_0^*. The transition is unaffected when cell stiffnesses K_A and K_P are allowed to vary. In contrast, introducing preferred cell areas or perimeters as tunable DOFs significantly alters the tissue's energy landscape, shifting p_0^* downwards. Learned spatial correlations in p_0 or a_0 can soften a tissue, and there are optimal values for the heterogeneity in p_0 ($\sigma_{p_0} \approx 0.15$) and a_0 ($\sigma_{a_0} \approx 0.3$) that lead to the largest shift of the transition.

Tunable DOFs have previously been introduced into networks that become rigid when the number of physical DOFs equals the number of physical constraints [1,3,4,30]. In contrast, vertex models are highly under-constrained and become rigid through geometric incompatibility [31]. Our finding that rigidity in these models is also strongly affected by tunable DOFs suggests that vertex models can be used to study epithelial mechanics in terms of double optimization processes.

It is well established that systems with fixed topology can learn intricate tasks [7]. While Hagh *et al.* [30] demonstrated that jammed particle packings subject to frequent rearrangements can learn to identify ultrastable states, it is difficult to tune arbitrary mechanical responses into *typical* jammed states because they are marginally stable to rearrangements [47]. Confluent epithelial tissues lie in an intermediate state between these two extremes—topological rearrangements, primarily in the form of T1 transitions, can occur but are not nearly as prevalent as in jammed packings. Our finding that preferred shape indices and cell areas effectively tune rigidity in vertex models suggests that introducing them as tunable DOFs could be a fruitful way of obtaining complex responses in systems that allow topological rearrangements.

The framework of physical learning with $\{p_{0,i}\}$ or $\{a_{0,i}\}$ as tunable DOFs could provide a new paradigm for understanding biological tissue mechanics. Individual cells can control cell- and molecular-scale properties, including the concentration of adhesion molecules and myosin motors, which in turn govern the preferred shape index locally [16,27] and alter effective cell-cell interactions. Our work indicates that tissues should be able to learn if they follow a global gradient closely enough. In other systems, it has been possible to identify local learning rules that project sufficiently onto the global gradient to allow double optimization [6,8,9,11,12]. It would be interesting to study whether local rules governing the dynamics of cell shapes and tensions that have already been proposed [17,48,49] project onto gradients of useful global cost functions, or conversely, to hypothesize cost functions for tissues and search for possible local learning rules that enable them to be minimized. More broadly, this framework could be useful for predicting how the dynamics of tissues arises from variation of cellular properties across developmental or evolutionary timescales.

ACKNOWLEDGMENTS

We thank Varda F. Hagh, R. Cameron Dennis, and Elizabeth Lawson-Keister for helpful discussions. M.L.M. and S.A. were supported by the Simons Foundation No. 454947, NSF-DMR-1951921, and SU's Orange Grid research computing cluster. I.T. and A.J.L. were supported by the NIH through Award 1-U01-CA-254886-01 and A.J.L. by the Simons Foundation No. 327939. A.J.L. thanks CCB at the Flatiron Institute, a division of the Simons Foundation, and the Isaac Newton Institute for Mathematical Sciences at Cambridge University (EPSRC Grant No. EP/R014601/1) for support and hospitality. I.T. acknowledges the CSIR-4PI Institute for providing the HPC facility.

DATA AVAILABILITY

The data that support the findings of this study are available in an accompanying Dryad repository at [50].

[1] C. P. Goodrich, A. J. Liu, and S. R. Nagel, The principle of independent bond-level response: Tuning by pruning to exploit disorder for global behavior, Phys. Rev. Lett. **114**, 225501 (2015).

[2] J. W. Rocks, N. Pashine, I. Bischofberger, C. P. Goodrich, A. J. Liu, and S. R. Nagel, Designing allostery-inspired response in mechanical networks, Proc. Natl. Acad. Sci. USA **114**, 2520 (2017).

[3] D. Hexner, A. J. Liu, and S. R. Nagel, Role of local response in manipulating the elastic properties of disordered solids by bond removal, Soft Matter **14**, 312 (2018).

[4] D. Hexner, A. J. Liu, and S. R. Nagel, Linking microscopic and macroscopic response in disordered solids, Phys. Rev. E **97**, 063001 (2018).

[5] J. W. Rocks, H. Ronellenfitsch, A. J. Liu, S. R. Nagel, and E. Katifori, Limits of multifunctionality in tunable networks, Proc. Natl. Acad. Sci. USA **116**, 2506 (2019).

[6] N. Pashine, D. Hexner, A. J. Liu, and S. R. Nagel, Directed aging, memory, and nature's greed, Sci. Adv. **5**, eaax4215 (2019).

[7] M. Stern and A. Murugan, Learning without neurons in physical systems, Annu. Rev. Condens. Matter Phys. **14**, 417 (2023).

[8] D. Hexner, N. Pashine, A. J. Liu, and S. R. Nagel, Effect of directed aging on nonlinear elasticity and memory formation in a material, Phys. Rev. Res. **2**, 043231 (2020).
[9] D. Hexner, A. J. Liu, and S. R. Nagel, Periodic training of creeping solids, Proc. Natl. Acad. Sci. USA **117**, 31690 (2020).
[10] B. Scellier and Y. Bengio, Equilibrium propagation: Bridging the gap between energy-based models and backpropagation, Front. Comput. Neurosci. **11**, 24 (2017).
[11] M. Stern, D. Hexner, J. W. Rocks, and A. J. Liu, Supervised learning in physical networks: From machine learning to learning machines, Phys. Rev. X **11**, 021045 (2021).
[12] S. Dillavou, M. Stern, A. J. Liu, and D. J. Durian, Demonstration of decentralized physics-driven learning, Phys. Rev. Appl. **18**, 014040 (2022).
[13] J. F. Wycoff, S. Dillavou, M. Stern, A. J. Liu, and D. J. Durian, Desynchronous learning in a physics-driven learning network, J. Chem. Phys. **156**, 144903 (2022).
[14] S. Dillavou, B. D. Beyer, M. Stern, M. Z. Miskin, A. J. Liu, and D. J. Durian, Machine learning without a processor: Emergent learning in a nonlinear electronic metamaterial, Proc. Natl. Acad. Sci. USA **121**, e2319718121 (2024).
[15] A. Mongera, P. Rowghanian, H. J. Gustafson, E. Shelton, D. A. Kealhofer, E. K. Carn, F. Serwane, A. A. Lucio, J. Giammona, and O. Campàs, A fluid-to-solid jamming transition underlies vertebrate body axis elongation, Nature (London) **561**, 401 (2018).
[16] X. Wang, M. Merkel, L. B. Sutter, G. Erdemci-Tandogan, M. Lisa Manning, and K. E. Kasza, Anisotropy links cell shapes to tissue flow during convergent extension, Proc. Natl. Acad. Sci. USA **117**, 13541 (2020).
[17] N. H. Claussen, F. Brauns, and B. I. Shraiman, A geometric tension dynamics model of epithelial convergent extension, Proc. Natl. Acad. Sci. USA **121**, e2321928121 (2024).
[18] G. Erdemci-Tandogan, M. J. Clark, J. D. Amack, and M. L. Manning, Tissue flow induces cell shape changes during organogenesis, Biophys. J. **115**, 2259 (2018).
[19] P. C. Sanematsu, G. Erdemci-Tandogan, H. Patel, E. M. Retzlaff, J. D. Amack, and M. L. Manning, 3D viscoelastic drag forces contribute to cell shape changes during organogenesis in the zebrafish embryo, Cells Dev. **168**, 203718 (2021).
[20] L. Hufnagel, A. A. Teleman, H. Rouault, S. M. Cohen, and B. I. Shraiman, On the mechanism of wing size determination in fly development, Proc. Natl. Acad. Sci. USA **104**, 3835 (2007).
[21] R. Farhadifar, J.-C. Röper, B. Aigouy, S. Eaton, and F. Jülicher, The influence of cell mechanics, cell-cell interactions, and proliferation on epithelial packing, Curr. Biol. **17**, 2095 (2007).
[22] J.-A. Park, J. H. Kim, D. Bi, J. A. Mitchel, N. T. Qazvini, K. Tantisira, C. Y. Park, M. McGill, S.-H. Kim, B. Gweon *et al.*, Unjamming and cell shape in the asthmatic airway epithelium, Nat. Mater. **14**, 1040 (2015).
[23] D. Bi, J. H. Lopez, J. M. Schwarz, and M. L. Manning, A density-independent rigidity transition in biological tissues, Nat. Phys. **11**, 1074 (2015).
[24] D. Bi, X. Yang, M. C. Marchetti, and M. L. Manning, Motility-driven glass and jamming transitions in biological tissues, Phys. Rev. X **6**, 021011 (2016).
[25] M. Chiang and D. Marenduzzo, Glass transitions in the cellular Potts model, Europhys. Lett. **116**, 28009 (2016).
[26] J. Devany, D. M. Sussman, T. Yamamoto, M. L. Manning, and M. L. Gardel, Cell cycle–dependent active stress drives epithelia remodeling, Proc. Natl. Acad. Sci. USA **118**, e1917853118 (2021).
[27] P. Sahu, D. M. Sussman, M. Rübsam, A. F. Mertz, V. Horsley, E. R. Dufresne, C. M. Niessen, M. C. Marchetti, M. L. Manning, and J. M. Schwarz, Small-scale demixing in confluent biological tissues, Soft Matter **16**, 3325 (2020).
[28] X. Wang, C. M. Cupo, S. Ostvar, A. D. Countryman, and K. E. Kasza, E-cadherin tunes tissue mechanical behavior before and during morphogenetic tissue flows, Curr. Biol. **34**, 3367 (2024).
[29] I. Tah, D. Haertter, J. M. Crawford, D. P. Kiehart, C. F. Schmidt, and A. J. Liu, A minimal vertex model explains how the amnioserosa avoids fluidization during *Drosophila* dorsal closure, Proc. Natl. Acad. Sci. USA **122**, e2322732121 (2025).
[30] V. F. Hagh, S. R. Nagel, A. J. Liu, M. L. Manning, and E. I. Corwin, Transient learning degrees of freedom for introducing function in materials, Proc. Natl. Acad. Sci. USA **119**, e2117622119 (2022).
[31] O. K. Damavandi, V. F. Hagh, C. D. Santangelo, and M. Lisa, Manning, Energetic rigidity. I. A unifying theory of mechanical stability, Phys. Rev. E **105**, 025003 (2022).
[32] A. Sharma, A. J. Licup, K. A. Jansen, R. Rens, M. Sheinman, G. H. Koenderink, and F. C. MacKintosh, Strain-controlled criticality governs the nonlinear mechanics of fibre networks, Nat. Phys. **12**, 584 (2016).
[33] J. L. Shivers, S. Arzash, A. Sharma, and F. C. MacKintosh, Scaling theory for mechanical critical behavior in fiber networks, Phys. Rev. Lett. **122**, 188003 (2019).
[34] M. Merkel, K. Baumgarten, B. P. Tighe, and M. L. Manning, A minimal-length approach unifies rigidity in underconstrained materials, Proc. Natl. Acad. Sci. USA **116**, 6560 (2019).
[35] S. Arzash, J. L. Shivers, and F. C. MacKintosh, Finite size effects in critical fiber networks, Soft Matter **16**, 6784 (2020).
[36] X. Li, A. Das, and D. Bi, Mechanical heterogeneity in tissues promotes rigidity and controls cellular invasion, Phys. Rev. Lett. **123**, 058101 (2019).
[37] H. Honda, Description of cellular patterns by Dirichlet domains: The two-dimensional case, J. Theor. Biol. **72**, 523 (1978).
[38] D. M. Sussman, cellGPU: Massively parallel simulations of dynamic vertex models, Comput. Phys. Commun. **219**, 400 (2017).
[39] E. Bitzek, P. Koskinen, F. Gähler, M. Moseler, and P. Gumbsch, Structural relaxation made simple, Phys. Rev. Lett. **97**, 170201 (2006).
[40] See Supplemental Material at http://link.aps.org/supplemental/10.1103/PhysRevResearch.7.013157 for details of the model, energy minimization algorithms, shear modulus calculation, tension percolation analysis, vibrational density of states, and comparison of emergent structural features in tissues.
[41] M. Merkel and M. L. Manning, A geometrically controlled rigidity transition in a model for confluent 3D tissues, New J. Phys. **20**, 022002 (2018).
[42] H. Bhaumik and D. Hexner, Mechanical regularization, Phys. Rev. Mater. **8**, L082601 (2024).
[43] M. Stern, A. J. Liu, and V. Balasubramanian, Physical effects of learning, Phys. Rev. E **109**, 024311 (2024).
[44] J. A. Zallen and R. Zallen, Cell-pattern disordering during convergent extension in *Drosophila*, J. Phys.: Condens. Matter **16**, S5073 (2004).

[45] X. Yang, D. Bi, M. Czajkowski, M. Merkel, M. L. Manning, and M. C. Marchetti, Correlating cell shape and cellular stress in motile confluent tissues, Proc. Natl. Acad. Sci. USA **114**, 12663 (2017).

[46] E. Teomy, D. A. Kessler, and H. Levine, Confluent and nonconfluent phases in a model of cell tissue, Phys. Rev. E **98**, 042418 (2018).

[47] B. Pisanty (private communication, 2023).

[48] M. F. Staddon, K. E. Cavanaugh, E. M. Munro, M. L. Gardel, and S. Banerjee, Mechanosensitive junction remodeling promotes robust epithelial morphogenesis, Biophys. J. **117**, 1739 (2019).

[49] N. Noll, M. Mani, I. Heemskerk, S. J. Streichan, and B. I. Shraiman, Active tension network model suggests an exotic mechanical state realized in epithelial tissues, Nat. Phys. **13**, 1221 (2017).

[50] https://doi.org/10.5061/dryad.k6djh9whr.